Dynamic *in situ* observations of electrical and structural changes in thin thermoelectric $(Bi_{0.15}Sb_{0.85})_2Te_3$ films

Katrin Bertram,[1,2,a)] Matthias Stordeur,[3] Frank Heyroth,[1] and Hartmut S. Leipner[1]
[1]*Interdisziplinäres Zentrum für Materialwissenschaften, Martin-Luther-Universität Halle-Wittenberg, Heinrich-Damerow-Str. 4, D-06120 Halle, Germany*
[2]*Angaris GmbH, Gr. Märkerstr. 18, D-06108 Halle, Germany*
[3]*HTC HighTech Consulting, Hallesche Str. 50, D-06122 Halle, Germany*

(Received 25 May 2009; accepted 16 August 2009; published online 24 September 2009)

Thin films of $(Bi_{0.15}Sb_{0.85})_2Te_3$ were prepared by dc magnetron sputter deposition on different substrates. It is well known that thermal treatment of as-deposited *p*-type $(Bi_{0.15}Sb_{0.85})_2Te_3$ films leads to an enhancement of the power factor. Whereas up to now only the initial (as deposited) and the final (after annealing) film stages have been investigated, here, the dynamic changes of sputter-deposited film properties have been observed by *in situ* measurements. The enhancement of the power factor shows a significant dependence on thermal treatment. The best thermoelectric films have been prepared at a substrate temperature of 170 °C, with a power factor of 24.4 $\mu W/(cm\ K^2)$. The changes in the Seebeck and Hall coefficients are caused by the enhancement in the Hall mobility after annealing. *In situ* x-ray diffractometry shows the generation of additional Te in dependence of the temperature. This is also confirmed by energy-dispersive x-ray microanalysis and the corresponding mapping in a scanning electron microscope. It is supposed that the locally well-defined Te enrichment is the reason for the improvement in the integral film transport properties. © *2009 American Institute of Physics*. [doi:10.1063/1.3225610]

I. INTRODUCTION

In addition to photovoltaics, thermoelectric energy conversion is a promising method for environment-friendly electricity production. Using the Seebeck effect in thermoelectric generators, renewable or waste heat fluxes driven by temperature gradients are directly transformed into electrical energy.[1] The thermoelectric figure-of-merit z of the materials used is the crucial parameter for the conversion efficiency. It is defined by $z=S^2\sigma/\kappa=P/\kappa$, where S is the Seebeck coefficient, σ is the electrical and κ is the thermal conductivity, and P is the so-called power factor.

It was found empirically that at least for all known thermoelectric bulk materials the relationship $zT<2$ (T is temperature) limits the efficiency of the energy conversion. Nevertheless, the search for new compounds with a higher thermoelectric figure-of-merit and their investigations continued undiminishedly.[2,3]

For devices in the operating range near room temperature (250–400 K), mixed crystals of the *p*-type solid solution $(Bi_{1-x}Sb_x)_2Te_3$ of the compounds Bi_2Te_3 and Sb_2Te_3 with $x\approx 0.8$ got the highest figure-of-merit[4,5] with $z_{max}\approx 3\times 10^{-3}\ K^{-1}$ in comparison with other materials. By nanostructuring,[6,7] the thermoelectric performance of Bi–Sb–Te bulk alloys could be enhanced recently to a value of $zT=1.4$ (Ref. 6) near a temperature of 400 K and $zT=1.56$ (Ref. 7) at 300 K.

A further ongoing trend is the miniaturization of thermoelectric devices such as generators or Peltier coolers up to the integration in electronic packages using the broad spectrum of thin film and nanotechnologies.[8–10] A wide application field for thin film generators is their use as power supplies for autonomous microsystems and sensors, e.g., for wireless data transfer.[9] Therefore, it is of topical interest to prepare thin film compound semiconductors and to study their thermoelectric properties. The deposition techniques used so far are, e.g., flash evaporation,[11] magnetron sputtering,[12,13] and coevaporation.[14]

It has been known from several authors[8,13,14] that annealing of the as-deposited films leads to a distinct enhancement of the power factor of the films and in this way also to an increase in the power output of the corresponding devices. It is obvious that partially the as-deposited films drastically change their electronic transport properties in connection with a change in the structure[8,13] after heat treatment. Whereas up to now only the initial (as-deposited) and the final (after annealing) film stages have been investigated, here the dynamical changes in the electrical conductivity during the annealing process have been observed by *in situ* measurements for the *p*-conductive thermoelectric compound $(Bi_{0.15}Sb_{0.85})_2Te_3$. The Seebeck and the Hall effects have been studied as well under stationary temperature conditions. In addition to the recording of these transport properties, the film structure and composition have been analyzed by *in situ* x-ray diffraction (XRD) in dependence of the temperature, field emission scanning electron microscopy (FESEM), and energy-dispersive x-ray microanalysis (EDX). Besides an extension of the experimental basis for a better understanding of the reasons for the changes of the film properties caused by heat treatment, the presented results could have a meaning for the optimization of the annealing process in the technological chain within the production pro-

[a)]Author to whom correspondence should be addressed. Electronic mail: katrin.bertram@cmat.uni-halle.de.

 © 2009 American Institute of Physics

Downloaded 29 Sep 2009 to 141.48.38.25. Redistribution subject to AIP license or copyright; see http://jap.aip.org/jap/copyright.jsp

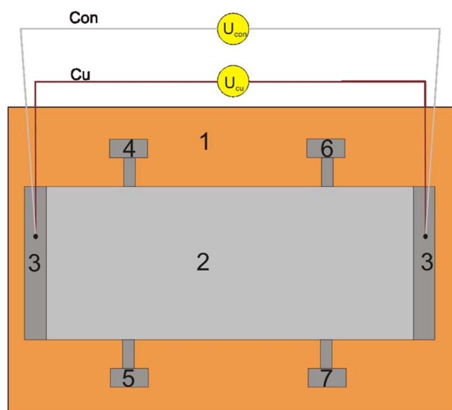

FIG. 1. (Color online) Scheme of a rectangular sample: (1) substrate, (2) thin thermoelectric film with a size of 3×15 mm^2, [(3)–(7)] nickel contacts for measuring the transport properties. The position of the thermocouples for the determination of the Seebeck coefficient is indicated by the indices Cu and Con.

cess of thermoelectric thin film devices[11] based on Bi_2Te_3/Sb_2Te_3 alloys.

II. FILM PREPARATION

Thin $(Bi_{0.15}Sb_{0.85})_2Te_3$ films were fabricated by dc magnetron sputter deposition on polyimide foils and Si/SiO_2 wafers at substrate temperatures of about 170 °C. According to the results described by Stölzer *et al.*,[15,16] the following target composition was used to achieve a stoichiometric film composition: $(Bi_{0.15}Sb_{0.85})_2Te_3$+20 at. % Te, with a purity of 5*N* of the basic material. The substrates were cleaned by ethanol and acetone. Residual contaminations on the substrates were eliminated prior to deposition by inverse sputter etching. Moreover, a better film adhesion on the substrate was achieved in this way.

Before deposition, the basic pressure in the vacuum chamber was lower than 1×10^{-4} Pa. All thin films were deposited with a sputtering rate of 6.17 nm/s. The substrate temperature was measured by a thermocouple lying directly under the substrate. Well-defined sample structures were prepared using a mask technique. Due to the different transport measurement methods carried out, two different sample geometries were used. Within one deposition run, a total of 22 thin film samples were produced with rectangular and squared shapes. The determination of the transport properties of the rectangular films required metallic contact pads, which were made of nickel. The layout of the rectangular samples is shown in Fig. 1. The squared samples were prepared with an edge length of 10 mm.

The Ni contacts with a thickness of about 3 μm for the rectangular samples were deposited by dc magnetron sputtering at room temperature. Three different film thicknesses (2, 6, and 20 μm) were investigated. The thickness of the films was determined by cross section FESEM.

The thermal treatment of the samples was performed in nitrogen atmosphere up to a maximum temperature of about 320 °C with a heating rate of 20 K/min. After reaching the chosen final temperature, the heater was turned off, and the sample was cooled down, without forced cooling.

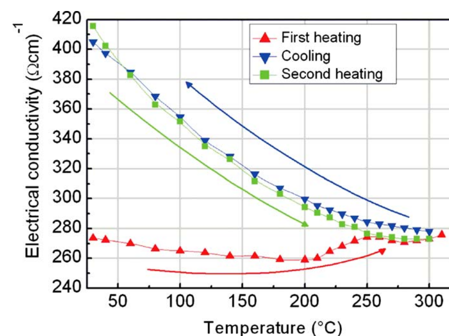

FIG. 2. (Color online) Electrical conductivity vs the temperature during thermal treatment of $(Bi_{0.15}Sb_{0.85})_2Te_3$ films with a thickness of 6 μm on a polyimide substrate. The arrows indicate the heating or cooling.

III. RESULTS

A. Measurement of transport properties

The electrical conductivity of thin films was measured in dependence of the temperature with two different methods. Squared samples were tested with the common four-probe method (two current and two voltage drop probes).

Rectangular samples were tested in a combined measurement setup for both the determination of the Seebeck coefficient and the electrical conductivity. The tests were carried out for measurement temperatures ranging from 20 up to 90 °C for as-deposited samples and after thermal treatment. The measurement of the electrical conductivity was carried out by a standard four-wire method to avoid the influence of the contact resistance. A constant current was applied at contact 3 in Fig. 1. The voltage was measured between contacts 4 and 6. The four-probe method and the four-wire method lead in the corresponding temperature range to very similar results.

Representative results of the dynamic *in situ* measurement of the electrical conductivity during thermal treatment are shown in Fig. 2. The first heating cycle of the as-deposited films shows typically three sections. From room temperature up to a temperature of about 200 °C, the electrical conductivity slightly decreases. When the temperature exceeds 200 °C, the electrical conductivity begins to increase up to a temperature of about 250 °C. A further increase in the temperature up to 320 °C shows no significant influence on the electrical conductivity. Afterwards, the temperature was lowered from about 320 °C to room temperature. In the temperature range between 320 and 260 °C, the electrical conductivity is nearly unchanged compared with the value of the first heating cycle. A further decrease in the temperature leads to a steadily rising electrical conductivity. This behavior was observed in all $(Bi_{0.15}Sb_{0.85})_2Te_3$ thin films. The enhancement of the electrical conductivity was found to be irreversible. This was confirmed by a second heating cycle from room temperature up to a temperature of about 320 °C. With rising temperature, the values of the electrical conductivity remain close to the results after the first cooling cycle at corresponding temperatures.

The behavior demonstrated in Fig. 2 has not been reported up to now for such thermoelectric films. Furthermore, it has to be noticed that only a thermal treatment above tem-

Downloaded 29 Sep 2009 to 141.48.38.25. Redistribution subject to AIP license or copyright; see http://jap.aip.org/jap/copyright.jsp

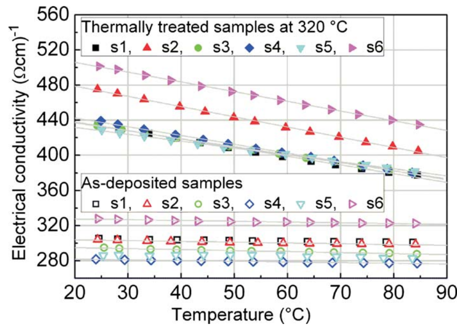

FIG. 3. (Color online) Electrical conductivity in dependence of temperature for 20 μm thick $(Bi_{0.15}Sb_{0.85})_2Te_3$ films on a polyimide substrate. *sN* stands for different samples.

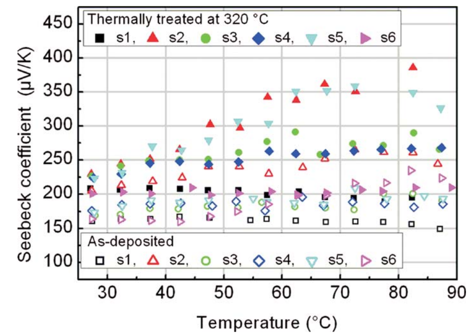

FIG. 4. (Color online) Seebeck coefficient in dependence of temperature for 20 μm thick $(Bi_{0.15}Sb_{0.85})_2Te_3$ films on a polyimide substrate. *sN* stands for different samples.

peratures of about 150 °C leads to an increase in the electrical conductivity. Measurements at samples on a Si/SiO_2 substrate show the same effect. Moreover, no dependence on film thickness was observed.

The electrical conductivity of the rectangular samples was measured before and after thermal treatment. The as-deposited samples show only a weak dependence of the electrical conductivity on temperature. All samples displayed in Fig. 3 were fabricated within one deposition run. Nevertheless, the electrical conductivity of these samples shows a variation between 280 and 330 $(\Omega\,\text{cm})^{-1}$. After thermal treatment, an increase in the electrical conductivity can be observed for all samples. Moreover, all films show after heat treatment a distinct decrease in the electrical conductivity with rising temperature. This corresponds to the measurements of the squared samples in the corresponding second heating temperature cycle (see Fig. 2).

In order to measure the Seebeck coefficient, a temperature difference of about 5 K was applied between contact 3 (Fig. 1). The thermovoltages of the copper-constantan thermocouples were measured and the Seebeck coefficient is calculated from the expression:[14]

$$S = \frac{U_{Cu}}{U_{Cu} - U_{Con}} S_{Cu\,Con} + S_{Cu}, \tag{1}$$

where U_{Cu} and U_{Con} are the thermovoltages between the copper wires and the constantan wires, respectively, and S_{Cu} and $S_{Cu\,Con}$ are the Seebeck coefficients of copper and of the copper-constantan couple, respectively (see Fig. 1).

The Seebeck coefficient of the as-deposited thin films varies between 161 and 206 μV/K at room temperature (Fig. 4). After thermal treatment at 320 °C, the Seebeck coefficient increases and scatters between 200 and 230 μV/K. In the tendency, the Seebeck coefficient is higher after thermal treatment. This behavior was found to be independent of the film thickness. A comparison of the values between individual samples *sN* confirms the expected tendency: the higher the electrical conductivity (see Fig. 3), the lower the Seebeck coefficient (see Fig. 4).

In addition to the measurement of the Seebeck coefficient and the electrical conductivity, the determination of the Hall coefficient provides information about changes in the transport parameters, such as carrier density and mobility. All Hall effect measurements were carried at room temperature before and after heat treatment. The electrical conductivity of the films was measured independent from the four-probe method again to calculate the Hall mobility within one measurement cycle. The electrical conductivity was measured between contacts 4 and 6 (see Fig. 1) and between 5 and 7. The Hall voltage U was measured between contacts 4 and 5 and between 6 and 7. To eliminate errors caused by possible Ohmic voltage drops between the Hall probes, it is sufficient to reverse the direction of the magnetic field and calculate the Hall coefficient ρ_H from the expression

$$\rho_H = \frac{(U_{+B} - U_{-B})d}{2IB}, \tag{2}$$

where U_{+B} and U_{-B} are the voltages under opposite directions of the magnetic field $+B$ and $-B$ with an orientation perpendicular to the sample surface. I is the current and d the thickness of the film. In Fig. 5, the results of the measurements for samples with different thicknesses and substrates are shown. The increase in the electrical conductivity due to the thermal treatment observed before can be confirmed with

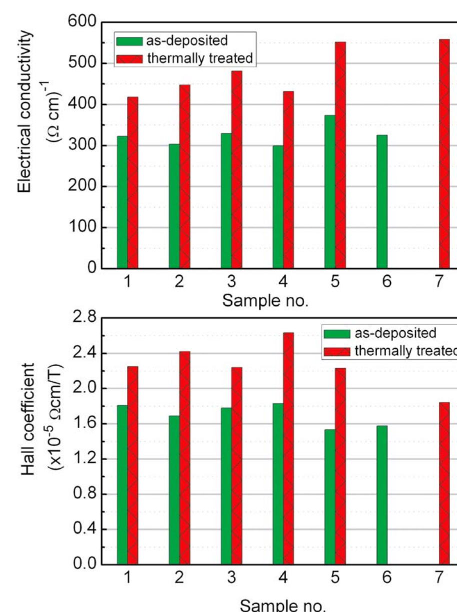

FIG. 5. (Color online) Electrical conductivity and Hall coefficient of thin $(Bi_{0.15}Sb_{0.85})_2Te_3$ films at room temperature, Sample nos. 1–3:6 μm thickness on a polyimide substrate, 4–5:20 μm on polyimide substrate, and 6–7:2 μm on a Si/SiO_2 substrate.

Downloaded 29 Sep 2009 to 141.48.38.25. Redistribution subject to AIP license or copyright; see http://jap.aip.org/jap/copyright.jsp

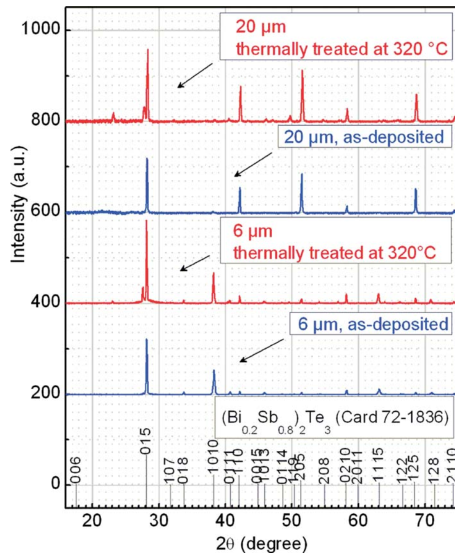

FIG. 6. (Color online) XRD pattern of $(Bi_{0.15}Sb_{0.85})_2Te_3$ thin films on polyimide substrate.

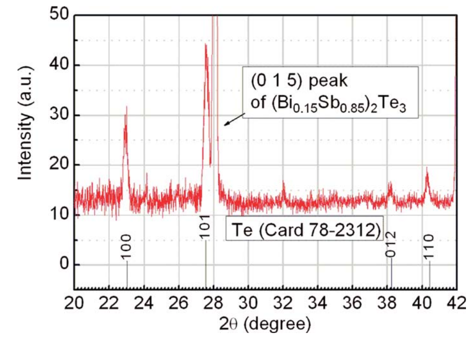

FIG. 7. (Color online) XRD pattern of a 20 μm $(Bi_{0.15}Sb_{0.85})_2Te_3$ thin film on polyimide substrate.

this method. Furthermore, all thin films posses a higher Hall coefficient after the thermal treatment, which is independent from the chosen substrate and the thickness of the films.

B. Film characterization by XRD, FESEM, and EDX

The morphology and the composition were investigated by means of XRD, FESEM, and EDX. The XRD measurements were performed at room temperature with a scan speed of 1/700 deg/s in the conventional $\theta-2\theta$ mode using a Siemens D5000 diffractometer (Cu $K\alpha$ radiation). For *in situ* measurements from room temperature up to 320 °C, the sample was placed on a heated sample goniometer in the diffractometer. An XRD pattern was taken every 10 °C at constant temperature with a scan speed of 1/125 deg/s.

Figure 6 shows the XRD results of the as-deposited and thermally treated films on polyimide substrate. From the comparison to the powder diffraction file,[17] the pattern of the as-deposited films can be attributed to the $(Bi_{0.15}Sb_{0.85})_2Te_3$ phase. All thin films show a texture before and after thermal treatment. Nevertheless, there are differences between films with different thicknesses. Only the distinct peaks which correspond to the (0 1 5) and (1 0 10) plane can be observed in as-deposited films with a thickness of 6 μm. Thicker films show numerous peaks with high intensity. Moreover, the (1 0 10) could not be observed. After thermal treatment, the peaks become sharper and gain in intensity, which is an indication of the grain growth. Additionally, some new peaks at an angle of 27.6° and 23.2° as well as some further small ones can be observed, which do not match the powder diffraction pattern of the $(Bi_{0.2}Sb_{0.8})_2Te_3$ phase. Figure 7 shows a closer look to the angular range where the additional peaks appear. Comparing with the powder diffraction file of tellurium,[18] these new peaks can be attributed to pure Te. The growing of the pure Te was investigated *in situ*. The angular scan was carried out close to the new (1 0 1) peak of the Te near the (0 1 5) peak of the mixed crystal. Figure 8 shows the result of the *in situ* heat treatment.

The peak of the Te begins to grow between 200 and 250 °C. It is fairly intense at the final temperature of 320 °C. Moreover, it can be seen that the peak of the Te is stable after cooling down. It is remarkable that the growth of the Te begins in the same temperature range where the increase in the electrical conductivity was to be observed with the four-probe method (Fig. 2).

Cross-sectional FESEM investigations of the thin films were performed on a Philips ESEM XL 30 FEG at an accelerating voltage of 12 kV. The structural differences between the as-deposited and thermally treated films apparent in the XRD patterns became also visible in FESEM micrographs (Fig. 9). The as-deposited films show a fine grain structure near the substrate, followed by a columnar pattern. The preferred orientation of the crystallites, which was observed in XRD, is also visible in the FESEM micrographs. The columnar structure can be assumed to be correlated with the (0 1 5) texture. After thermal treatment, the fine grain sized structure near the substrate remained despite the structural changes. However, the film became porous [Fig. 9(b)]. The overall elemental composition of the films was determined by means of EDX (Table I). It was found that the composition of the

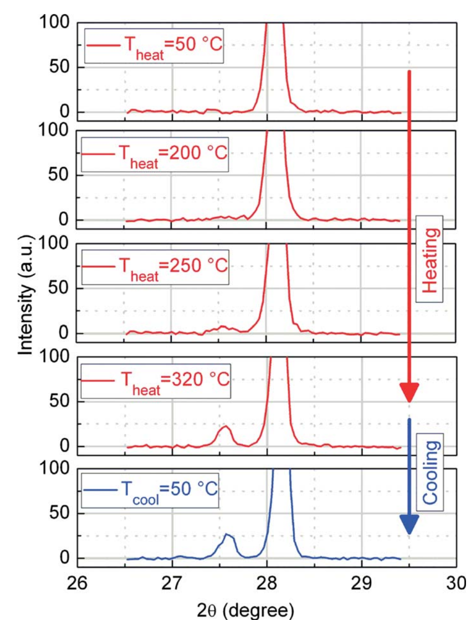

FIG. 8. (Color online) *In situ* XRD pattern of a 20 μm thick $(Bi_{0.15}Sb_{0.85})_2Te_3$ film on polyimide substrate during heating and cooling.

Downloaded 29 Sep 2009 to 141.48.38.25. Redistribution subject to AIP license or copyright; see http://jap.aip.org/jap/copyright.jsp

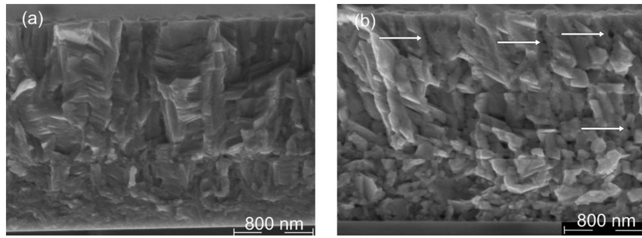

FIG. 9. Cross-sectional FESEM micrographs of a 2 μm $(Bi_{0.15}Sb_{0.85})_2Te_3$ thin film on Si/SiO_2 substrate: (a) as-deposited and (b) after thermal treatment at 320 °C, arrows indicate the porosity.

films slightly deviates from the stoichiometry. The overall composition remained nearly unchanged by thermal treatment.

The samples for EDX mappings were prepared in a sandwichlike arrangement. Thin films grown on Si/SiO_2 substrates were embedded between two pieces of silicon with epoxy resin. A cross section was prepared by cutting and polishing. For the EDX signal of each element and the background, a separate channel was defined. Each mapping was taken from the over all cross section over a sample length of 7.78 μm. The analysis of EDX mappings was carried out by subtracting the background signal and averaging over all positions parallel to the substrate in order to get the elemental distribution in the growth direction.

The result of the EDX measurements is given in Fig. 10(a). The distribution of the elements Te, Sb, and Bi shows no distinct differences in the as-deposited films. The mapping of thermally treated film confirms the XRD measurements. The analysis of the EDX mapping in Fig. 10(b) show a lamella with an increase in the tellurium concentration, accompanied by a lower concentration of bismuth and antimony. EDX mapping using the tellurium L edge (Fig. 11) corroborates the result. The Te is located in between the region with fine grains close to the substrate and the columnar structure at the top of the film.

IV. DISCUSSION

With the increase in the electrical conductivity σ and the Seebeck coefficient S, the power factor benefits from the thermal treatment. Figure 12 shows the power factor of different samples before and after thermal treatment.

The power factor of the as-deposited films varied between 7.1 and 13.4 $\mu W/(K^2\,cm^1)$. These values are higher than results of films deposited at room temperature reported previously.[13] The influence of substrate temperature was investigated in coevaporated films.[14] It was found that a higher substrate temperature lead to a higher power factor. The

TABLE I. EDX analysis of thin films (representative for all films).

Element	EDX (at. %)	Expected from stoichiometry (at. %)
Te	59.25 ± 1.19	60
Sb	33.07 ± 0.60	34
Bi	7.68 ± 0.04	6

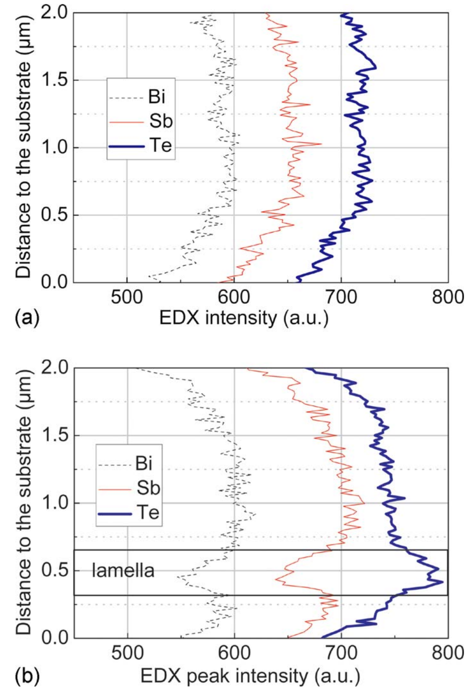

FIG. 10. (Color online) EDX mapping of a 2 μm $(Bi_{0.15}Sb_{0.85})_2Te_3$ thin film on Si/SiO_2 substrate: (a) as-deposited and (b) after thermal treatment at 320 °C.

highest power factor of 24.4 $\mu W/(K^2\,cm^1)$ obtained after thermal treatment at 320 °C is higher than other reported values[13] and close to the maximum power factor of 36 $\mu W/(K^2\,cm^1)$ reported for deposition at higher substrate temperatures.[8]

The values calculated for the Hall mobility μ and the carrier concentration p are shown in Fig. 13. It is remarkable that the films posses a lower carrier concentration after thermal treatment. Simultaneously, the Hall mobility has been increased by the factor of about 2 after the thermal treatment. The Seebeck coefficient relates to the carrier density in tendency by $S \propto p^{-2/3}$. The correlation of the Hall mobility and the electrical conductivity is given by $\sigma = e\mu p$, where e is the unit charge. This explains the simultaneous increase in the electrical conductivity and the Seebeck coefficient after thermal treatment.

The lower carrier concentration after thermal treatment benefits the Seebeck coefficient. The enhancement of the Hall mobility is higher than the decrease in the carrier concentration. Consequently, the electrical conductivity increases by the thermal treatment.

Investigations of the structural changes have shown a

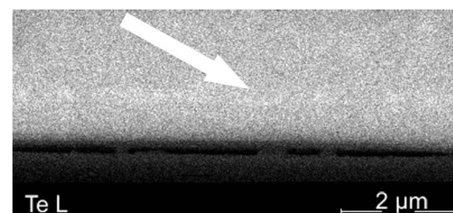

FIG. 11. EDX mapping of tellurium of a 2 μm $(Bi_{0.15}Sb_{0.85})_2Te_3$ thin film on Si/SiO_2 substrate after thermal treatment at 320 °C. The arrow points at the lamella.

Downloaded 29 Sep 2009 to 141.48.38.25. Redistribution subject to AIP license or copyright; see http://jap.aip.org/jap/copyright.jsp

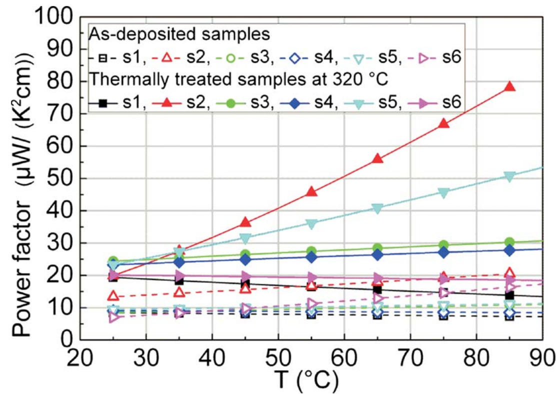

FIG. 12. (Color online) Power factor as a function of the temperature for $(Bi_{0.15}Sb_{0.85})_2Te_3$ samples with a film thickness of 20 μm on polyimide substrate.

grain growth and the formation of locally well-defined Te precipitates. These two conditions are related to the enhancement of the integral transport properties.

Furthermore, it is supposed that the pure Te is a crucial factor for the improvement of the power factor, since the increase in the electrical conductivity was observed in the same temperature range where the Te started to grow (see Figs. 2 and 8). The formation of the Te precipitates is located between the fine crystalline and the columnar regions (see Figs. 9–11). It was reported[6,19] that nanograined bulk $Bi_xSb_{2-x}Te_3$ showed pure tellurium precipitates with diameters ranging between 5 and 50 nm.

The (0 1 5) reflexion (see Fig. 6) observed in the XRD pattern indicated that the c-axis of most crystallites is tilted of about 11.3° to the substrate surface. In contrast with other authors,[14,20] crystallites with the orientation of the c-axis perpendicular to the substrate surface were not found, since the XRD pattern had shown no appearance of the (0 0 6) reflexion. For the explanation of the correlation between the decrease in the carrier concentration and the growth of the Te after thermal treatment, it is necessary to look at the characteristics of a single crystal. The single crystal compound semiconductors Bi_2Te_3 and Sb_2Te_3 and the ternary mixed crystal system $(Bi_{1-x}Sb_x)Te_3$ $(0 \leq x \leq 1)$ have a fivefold layer sequence along the trigonal c-axis: $Te^1YTe^2YTe^1$ (Y=Bi, Sb; Te^1 and Te^2 denote the different Te stacking positions). From

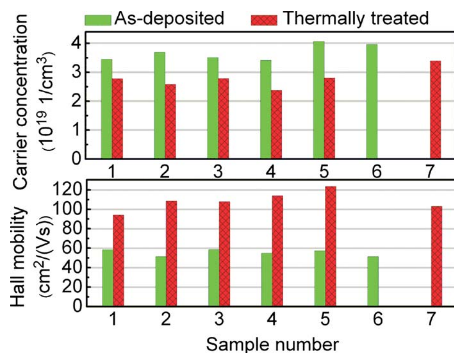

FIG. 13. (Color online) Carrier concentration and Hall mobility of thin films at room temperature, Sample nos. 1–3: 6 μm on polyimide substrate, 4–5: 20 μm on polyimide substrate and 6–7: 2 μm on Si/SiO_2 substrate.

literature,[21] it is known that the carrier concentration is related to the concentration of antisite defects. In the case of Sb_2Te_3- and Sb_2Te_3-rich crystals, an Sb atom on the Te^2 position generates a hole. Electromigration experiments of copper and the doping properties of Pb and Ge in Sb_2Te_3 showed that, besides the antisite defects, additionally defects exist in the Sb sublattice, where Te occupy an Sb site with donor behavior.[22,23] It is assumed that simultaneously with the grain growth, Te is able to diffuse during the thermal treatment through the polycrystalline film, and thereby some Te atoms occupy Sb sites in the sublattice. This could lead to the observed decrease in the carrier concentration. A more detailed analysis of the structure by means of TEM and the investigation of the thermal conductivity in future studies would lead to a better understanding of the influence of the Te precipitates.

ACKNOWLEDGMENTS

The author would like to thank C. Eisenschmidt for supporting the XRD measurements.

[1]G. W. Crabtree and N. S. Lewis, Phys. Today **60**, 37 (2007).
[2]S. R. Brown, S. M. Kauzlarich, F. Gascoin, and G. J. Snyder, Chem. Mater. **18**, 1873 (2006).
[3]D. I. Bilc, S. D. Mahanti, and M. G. Kanatzidis, Phys. Rev. B **74**, 125202 (2006).
[4]M. Stordeur, Phys Status Solidi B **161**, 831 (1990).
[5]M. Stordeur, in *Handbook of Thermoelectrics*, edited by D. M. Rowe (CRC, Boca Raton, New York, London, Tokyo, 1995), p. 239.
[6]B. Poudel, Q. Hao, Y. Ma, Y. Lan, A. Minnich, B. Yu, X. Yan, D. Wang, A. Muto, D. Vashaee, X. Chen, J. Liu, M. S. Dresselhaus, G. Chen, and Z. Ren, Science **320**, 634 (2008).
[7]W. Xie, X. Tang, Y. Yan, Q. Zhang, and T. M. Tritt, Proceedings of the 28th International Conference/7th European Conference on Thermoelectrics, Freiburg, Germany 26–30 July, 2009, p. 55.
[8]M. Stordeur and G. Willers, Proceedings of the Second European Conference on Thermoelectrics, Krakow, Poland, 15–17 September 2004.
[9]N. S. Hudak and G. G. Amatucci, J. Appl. Phys. **103**, 101301 (2008).
[10]I. Chowdhury, R. Prasher, K. Lofgreen, G. Chrysler, S. Narasimhan, R. Mahajan, D. Koester, R. Alley, and R. Venkatasubramanian, Nat. Nanotechnol. **4**, 235 (2008).
[11]X. Duan, J. Yang, W. Zhu, X. A. Fan, and S. Q. Bao, J. Phys. D **39**, 5064 (2006).
[12]H. Böttner, J. Nurnus, and A. Schubert, in *Thermoelectrics Handbook Macro to Nano*, edited by D. M. Rowe (Taylor & Francis, Boca Raton, London, New York, 2005), Chap. 46.
[13]D. Bourgault, C. G. Garampon, N. Caillaut, L. Carbone, and J. A. Aymami, Thin Solid Films **516**, 8579 (2008).
[14]L. W. da Silva, M. Kaviany, and C. Uhre, J. Appl. Phys. **97**, 114903 (2005).
[15]M. Stölzer, V. Bechstein, and J. Meusel, Proceedings of the 15th International Conference on Thermoelectrics, Pasadena, 26–29 March, 1996, p 422.
[16]M. Stölzer, V. Bechstein, and J. Meusel, Proceedings of the 16th International Conference on Thermoelectrics, Dresden, Germany, 26–29 August, 1997, p. 93.
[17]Powder Diffraction File No. 72-1836, Joint Committee of Powder Diffraction Standards (1993–1994).
[18]Powder Diffraction File No. 78-2312, Joint Committee of Powder Diffraction Standards (1993–1994).
[19]Y. Lan, B. Poudel, Y. Ma, D. Wang, M. S. Dresselhaus, G. Chen, and Z. Ren, Nano Lett. **9**(4), 1419 (2009).
[20]M. Takashiri, K. Miyazaki, and H. Tsukamoto, Thin Solid Films **516**, 6336 (2008).
[21]J. R. Drabble and C. H. L. Goodman, J. Phys. Chem. Solids **5**, 142 (1958).
[22]A. Priemuth, Phys. Status Solidi A **67**, 505 (1981).
[23]H. Süssmann, A. Priemuth, and U. Pröhl, Phys. Status Solidi A **82**(2), 561 (1984).

Downloaded 29 Sep 2009 to 141.48.38.25. Redistribution subject to AIP license or copyright; see http://jap.aip.org/jap/copyright.jsp